Assessment of a Silicon Quantum Dot Spin Qubit Environment via Noise Spectroscopy

K. W. Chan,[1,*] W. Huang,[1] C. H. Yang,[1] J. C. C. Hwang,[1] B. Hensen,[1] T. Tanttu,[1] F. E. Hudson,[1] K. M. Itoh,[2] A. Laucht,[1] A. Morello,[1] and A. S. Dzurak[1,†]

[1] *Centre for Quantum Computation and Communication Technology, School of Electrical Engineering and Telecommunications, The University of New South Wales, Sydney, New South Wales 2052, Australia*

[2] *School of Fundamental Science and Technology, Keio University, 3-14-1 Hiyoshi, Kohoku-ku, Yokohama 223-8522, Japan*

(Received 24 May 2018; revised manuscript received 6 July 2018; published 5 October 2018)

Preserving coherence long enough to perform meaningful calculations is one of the major challenges on the pathway to large-scale quantum-computer implementations. Noise coupled in from the environment is the main factor contributing to decoherence but can be mitigated via engineering design and control solutions. However, this is possible only after acquisition of a thorough understanding of the dominant noise sources and their spectrum. In the work reported here, we use a silicon quantum dot spin qubit as a metrological device to study the noise environment experienced by the qubit. We compare the sensitivity of this qubit to electrical noise with that of an implanted silicon-donor qubit in the same environment and measurement setup. Our results show that, as expected, a quantum dot spin qubit is more sensitive to electrical noise than a donor spin qubit due to the larger Stark shift, and the noise-spectroscopy data show pronounced charge-noise contributions at intermediate frequencies (2–20 kHz).

DOI: 10.1103/PhysRevApplied.10.044017

I. INTRODUCTION

Spin-based quantum dot qubits [1] in semiconductors show promise for scalable quantum-information processing due to their compatibility with well-established semiconductor manufacturing technologies. Extremely long electron spin-coherence times have been demonstrated in spin qubits fabricated on isotopically purified silicon [2–5], with control and read-out fidelities exceeding fault-tolerance thresholds [3,6]. Two-qubit logic gates [7–10] based on silicon quantum dots have also been demonstrated as a consequence of these advancements. Scaling up to larger multiqubit systems, however, requires a more-stringent engineering of the qubits' electromagnetic environment such that the collective fault-tolerance threshold is maintained for the implementation of surface code error-correction protocols [11]. This demands a detailed understanding of the possible sources of noise that cause decoherence at the very least.

Noise spectroscopy is a valuable and necessary tool in building understanding of the noise sources present. As part of the effort toward scaling up qubit systems, noise spectroscopy measurement has been undertaken for superconducting [12], ion-trap [13] and diamond-nitrogen-vacancy-center [14] qubits. Noise spectroscopy for spin-based quantum computing in silicon has been performed for an implanted phosphorus-donor in silicon (Si:P) [2] qubit and a SiGe quantum dot [6] spin qubit. Here we use a silicon metal-oxide-semiconductor (SiMOS) quantum dot spin qubit as a probe to enable noise spectroscopy via Carr-Purcell-Meiboom-Gill (CPMG) dynamical decoupling pulse sequences [15,16]. We start by comprehensive characterization of the qubit, which includes coherence-time measurements and randomized benchmarking of the single-qubit Clifford-gate control fidelities.

II. DEVICE ARCHITECTURE AND CHARACTERIZATION

Figure 1(a) shows a scanning electron micrograph of an identical device fabricated on an isotopically enriched 900-nm ^{28}Si epilayer [17] with an 800-ppm residual concentration of ^{29}Si. This device is fabricated on the basis of our previously reported aluminium-gate-stacked architecture [18,19], with the distinction of using bilayer PMMA/copolymer resist to ease the metal liftoff process. The single-electron transistor (SET) is a charge sensor [20] used to read out the charge occupancy and electron spin state of the confined quantum dots under gates G1–G3. Gate GT acts as a tunnel barrier for the loading of electrons into the quantum dots from the reservoir gate (RES).

*ckwai85@gmail.com
†a.dzurak@unsw.edu.au

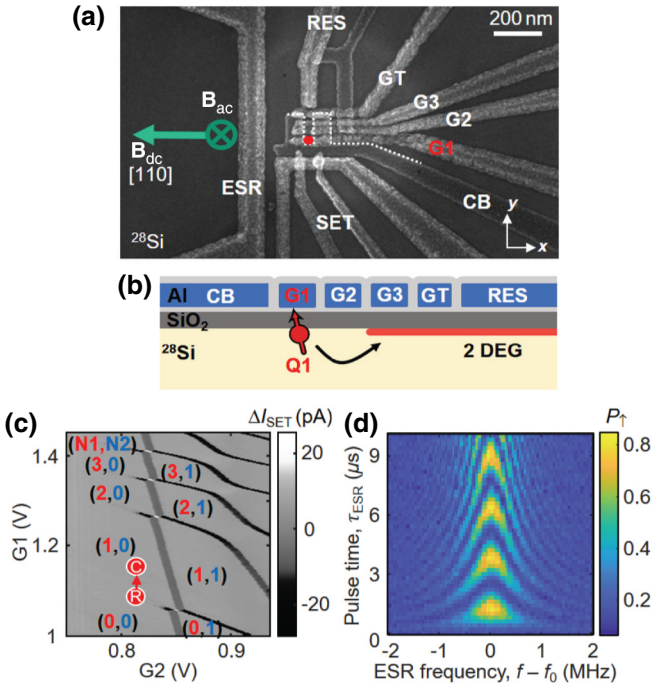

FIG. 1. (a) Scanning electron micrograph of a SiMOS qubit device identical to the one studied here. The quantum dot confinement gate (CB) is marked with a dotted white line. Each quantum dot is confined in a 40×40 nm^2 area underneath gates G1–G3. (b) Cross section of (a) along the y axis of the qubit marked with a red dot (not to scale). In this paper, we report on the data obtained from qubit Q1, formed underneath gate G1, as depicted by the red dot. (c) Charge-stability diagram of a double-quantum-dot system confined under gates G1 and G2. (d) Rabi-chevron map showing qubit spin-up probability as a function of ESR detuning frequency, $f - f_0$, and ESR pulse time, τ_{ESR}. Here the ESR frequency is $f_0 = 38.7765$ GHz, $\mathbf{B}_{dc} = 1.4$ T, and the applied source microwave power $P_{ESR} = 5$ dBm. From these results, we extract the electron Landé g factor to be 1.9789.

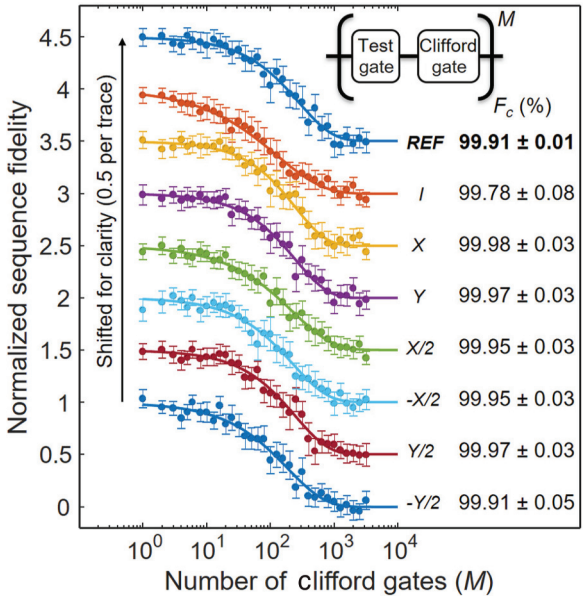

FIG. 2. Randomized benchmarking of Clifford gates to determine the control fidelity of our qubit. The performance of each Clifford gate is tested by interleaving them with random Clifford gates. The Clifford-gate control fidelity of this device is 99.83%. The data are vertically shifted by 0.5 per trace for clarity. All error bars represent 95% confidence intervals taken from the exponential fits used to extract the control fidelity.

Gates G1–G3 are used to tune the electron occupancies. A dc magnetic field $\mathbf{B}_{dc}$ of 1.4 T is applied to Zeeman split the electron spin states to form the qubit eigenstates. The electron spin state is manipulated by use of the electron-spin-resonance (ESR) microwave line to produce a perpendicular ac magnetic field $\mathbf{B}_{ac}$ at microwave frequency f_0. The directions of both magnetic fields, $\mathbf{B}_{dc}$ and $\mathbf{B}_{ac}$, are indicated in Fig. 1(a). Figure 1(b) shows a schematic cross section of the device along the y axis of the qubit, marked with a red dot in Fig. 1(a). The red region underneath the reservoir gate illustrates a 2DEG formed with positive bias voltage, and extends to a nearby phosphorus-doped ohmic region.

Figure 1(c) depicts the stability diagram showing the charge transitions on a double-dot system that is electrostatically confined under gates G1 and G2. The electron occupancies are labeled in each Coulomb blockaded region as (N1,N2), with N1 (N2) representing the number of electrons under gate G1 (G2). In this experiment, the double dot is effectively configured as a single dot by operating near the $(0, 0)$–$(1, 0)$ charge transition. The qubit Q1 control (C) and read-out (R) positions are labeled in red. Detailed reports on the ESR measurement technique and setup are presented in Ref. [3]. The measured Rabi-chevron pattern is depicted in Fig. 1(d). The high-quality chevron shows excellent control of the electron spin, with an extracted π-pulse time of 1.28 μs. With use of the single-shot spin to charge conversion technique [20,21], all experimental data shown are obtained with the electron-reservoir tunnel rate tuned to approximately 100 μs with at least 100 single-shot measurements for each data point. For this qubit, we measure a spin relaxation time $T_1 \approx 1$ s and a Ramsey [22] dephasing time $T_2^* = 33 \pm 8$ μs (data not shown). In addition, we measure the routinely reported coherence times $T_2^H = 401 \pm 42$ μs, $T_2^{CP} = 1.5 \pm 0.2$ ms ($N = 7$ pulses), and $T_2^{CPMG} = 6.7 \pm 2.9$ ms ($N = 122$ pulses) using Hahn echo [23], Carr-Purcell [24], and Carr-Purcell-Meiboom-Gill [25] pulse sequences, respectively.

III. RANDOMIZED BENCHMARKING

We perform randomized benchmarking [26] of Clifford gates to determine our control fidelity using standard microwave square pulses as part of the characterization.

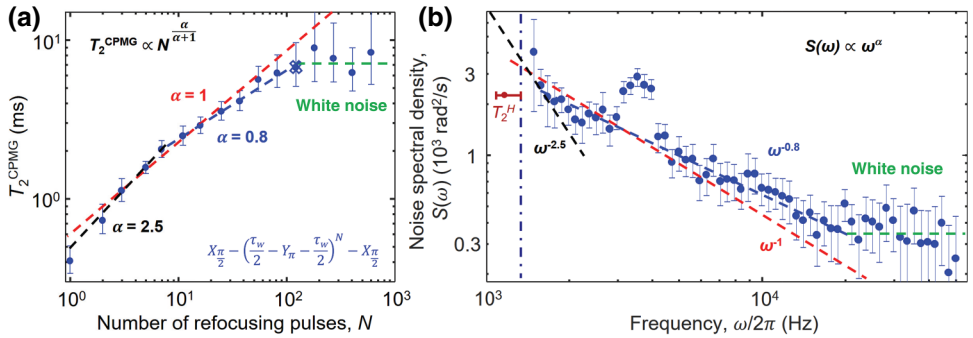

FIG. 3. (a) Qubit CPMG coherence time as a function of the number of refocusing pulses N. The maximum T_2^{CPMG} is 6.7 ms as shown by the data point marked with a cross. (b) Noise spectrum of a SiMOS quantum dot spin qubit. The noise power spectral density $S(\omega)$ is calculated from the T_2^S data fitted to an exponential decay of the form $P(t) = P_0\exp[(-t/T_2^S)^n] + P_\infty$ for different wait times τ_w between the Y_π pulses. We observe a colored noise spectrum with an exponent of $\alpha = -2.5$ for $f < 2$ kHz. At intermediate frequencies ($f = 2$–20 kHz), our noise is dominated by an exponent of $\alpha = -0.8$ to -1, very close to $1/f$, which we attribute to charge noise. We also observe a pronounced peak in the spectrum at $f \approx 3.6$ kHz, which is caused by measurement electronics. At high frequencies ($f > 20$ kHz), our white-noise floor is 350 rad^2/s. All error bars represent 95% confidence intervals from the exponential fits used to extract the decay times.

Figure 2 displays the converted spin-up probability to control fidelity as a function of the number of Clifford-gate operations M. All of the data are normalized from the fidelity obtained at $M = 1$ and expected decay at large M, with 0.55 visibility, limited by read-out and initialization errors. This means that a fidelity of zero is defined as a completely random state. The performance of each Clifford gate is tested by interleaving them with random Clifford gates. The sequence fidelity decays over more than several hundred pulses. A π-pulse time of 1.75 μs and a wait time of 100 ns between consecutive gates are used in each measurement trace. The Clifford-gate fidelity [27] is 99.83%, which gives a primitive-gate fidelity $F_{\mathrm{ref}} =$ 99.91% based on a gate length 1/1.875 of the average Clifford-gate length. In addition to exceeding the threshold required for quantum-error correction with use of surface codes [28], this is also a factor of 4 reduction in error rate in comparison with our previous best fidelity record reported in Ref. [3]. We attribute this improvement to the use of the I-Q modulation of a vector microwave signal generator, which has a higher phase-control bandwidth than the analog phase-modulation mode used in Ref. [3]. In addition, we implement ESR frequency feedback in our measurement code to keep track of and correct the drift in f_0 [29], possibly due to drift in $\mathbf{B}_{\mathrm{dc}}$ and random charge or dc-voltage-supply fluctuations. Our achievement of a high control fidelity suggests that our coherence times and noise-spectroscopy measurements are not limited by the ESR control pulses.

IV. NOISE SPECTROSCOPY

Figure 3(a) shows a plot of the CPMG coherence times versus the number of refocusing pulses N. The corresponding pulse sequences are shown at the bottom right, with Y_π denoting a π rotation on the y axis of the Bloch sphere and τ_w the wait time between the π pulses. The coherence time can be extended by increase of N until it saturates at $N = 122$. The dashed lines are the power-law dependence of the noise spectrum, and are explained later. Figure 3(b) shows the noise spectrum of our silicon quantum dot qubit. We use our qubit as a noise probe to measure the noise power spectral densities $S(\omega)$ using CPMG pulse sequences [15] as demonstrated for a phosphorus-donor qubit system earlier [2]. CPMG pulse sequences is a spin-refocusing technique used to remove dephasing effects of low-frequency transverse-magnetic noise. Thus, in noise-spectroscopy measurements, the CPMG sequences act as a bandpass filter, selectively choosing the portion of the noise spectrum that couples to the qubit. $S(\omega)$ is calculated from the T_2^S data fitted to an exponential decay of the form $P(t) = P_0\exp[(-t/T_2^S)^n] + P_\infty$ for different τ_w between the Y_π pulses. T_2^S is the electron spin-coherence time measured while τ_w is kept constant and the number of pulses in a CPMG sequence is progressively increased until the spin-up probabilities decay completely. For each τ_w, we compute $S(\omega) = \pi^2/4T_2^S(\omega)$, and the wait time is translated into frequency by $f = 1/2\tau_w$ [2,16]. The noise spectroscopy is limited to 1.3–50 kHz because at low frequency τ_w between the Y_π pulses approaches T_2^H and at high frequency we are bound by the shortest τ_w (10 μs) that is experimentally available.

In Fig. 3(b), we observe a colored noise spectrum with an exponent of α, closely reminiscent of $\alpha = -2.5$ for $f < 2$ kHz. The dashed black line is a plot of the function $C_1/\omega^{2.5}$, with $C_1 = 3 \times 10^{13}$. In the Si:P qubit [2], this noise was attributed to the drift and fluctuations of $\mathbf{B}_{\mathrm{dc}}$ in the superconducting-magnet coils. Since

both experiments are conducted in the same cryomagnetic system, the fact that their values are different ($C_1 = 6 \times 10^{11}$ in Ref. [2]) hints that the fluctuations of $\mathbf{B}_{dc}$ in the superconducting-magnet coils may not be the cause of the $1/f^{2.5}$ noise seen in the quantum dot and Si:P qubit systems at low frequency. At frequencies $f = 2$–20 kHz, our qubit noise follows the exponent of $\alpha = -0.8$ to -1, resembling the nature of $1/f$ charge noise [6,30–33]. The dashed red (blue) line is a plot of the function C_2/ω ($C_3/\omega^{0.8}$), with $C_2 = 3 \times 10^7$ ($C_3 = 4 \times 10^6$). These dashed lines are guides for the eye. At high frequencies ($f > 20$ kHz), the white-noise floor is 350 rad^2/s, marked with a dashed green line. In Fig. 3(a), according to the power law of the noise, the coherence time T_2^{CPMG} is expected to scale according to the noise color in Fig. 3(b) as $T_2 \propto N^{\alpha/(\alpha+1)}$ [34]. The dashed lines in Fig. 3(a) are plotted with corresponding α values to reflect the power-law dependence of the noise spectrum. The data show excellent agreement with the measured dependencies.

In Fig. 3(b), we also observe a pronounced peak in the spectrum at $f \approx 3.6$ kHz, which is a feature not observed in the Si:P qubit experiments [2]. After thorough investigation, we find that this peak is most likely caused by the dc voltage sources (SIM928) used to bias the qubit device. In the Appendix, we report measurements of the noise spectrum of the SIM928 voltage source and observe a prominent peak at the exact same frequency, $f \approx 3.6$ kHz, and attribute this to be the cause of the peak observed in the noise spectrum in Fig. 3(b).

Figure 4(a) shows the measurement of the Stark shift of the g factor experienced by qubit G1 as a function of G1 and G2 gate voltages. The electric field creates a Stark shift of the electron g factor due to finite spin-orbit coupling [3,35]. From the two-dimensional map, we extract the voltage-induced Stark shift from G1 and G2 to be $df/dV_{G1} = -36.21$ MHz/V and $df/dV_{G2} = -22.88$ MHz/V, respectively. Our Stark shifts are comparable with those of other reported silicon quantum dot qubits [3,36] and are much larger than the -2.27 MHz/V reported for the Si:P qubit [37]. The enhanced Stark shift caused by a less tightly confined quantum dot qubit renders the quantum dot more sensitive to electrical noise than the Si:P qubit. This is obvious from the $1/f$ dependence in the noise spectrum at intermediate frequencies and the higher white-noise floor (350 rad^2/s vs 10 rad^2/s for the Si:P qubit [2]). A detailed analysis of the Stark-shift effect modulated by the electric field on a silicon quantum dot spin qubit is provided in Ref. [35].

By applying a sinusoidal tone on gate G2 to deterministically Stark shift the qubit's frequency, we can verify our noise-spectroscopy measurement technique and setup. We set the tone frequency to 20 kHz as it corresponds to the onset where $S(\omega)$ is saturated by the white noise. Figure 4(b) shows the measured qubit spin-up

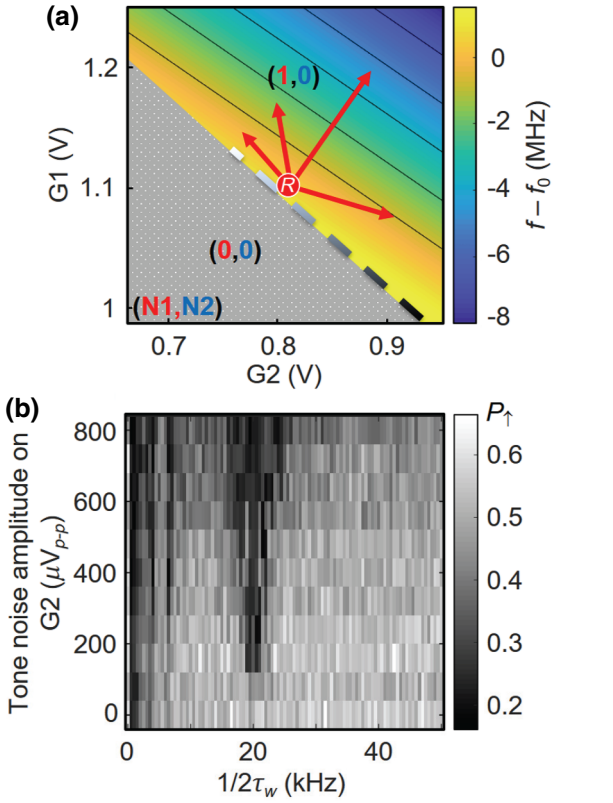

FIG. 4. (a) Stark shift experienced by qubit G1 as a function of G1 and G2 gate voltages. The ESR frequencies are measured at different gate spaces with 8-mV step size and are extrapolated linearly as shown in the two-dimensional map. Here $f_0 = 38.7765$ GHz. From the results, we fit the qubit G1 Stark shift to be $df/dV_{G1} = -36.21$ MHz/V and $df/dV_{G2} = -22.88$ MHz/V. (b) CPMG noise spectrum obtained with application of a 20-kHz sinusoidal tone as a function of its amplitude on gate G2 on the y axis. The x axis is translated into frequency from the CPMG wait time, and all data are taken with a fixed total precession time. The results elucidate significantly lower spin-up probability at a tone frequency starting from 160 μV peak to peak. This is a verification of our noise-spectroscopy measurement technique and setup.

probability after CPMG pulse sequences with different τ_w, converted into a unit of frequency on the x axis, and repeated with different tone amplitudes. The results elucidate significantly lower spin-up probability at the tone frequency starting from approximately 160 μV peak to peak. Despite the much larger Stark shift for the quantum dot qubit, this value is comparable to the approximately 200 μV peak to peak in the Si:P qubit system, as the tone needs to overcome an approximately-35-times-higher noise floor before it becomes visible. Lower spin-up probabilities are also observed in the third (6.66 kHz) and fifth (4 kHz) harmonics of 20 kHz but not in the even harmonics as their effect has been suppressed by the CPMG filter function [38].

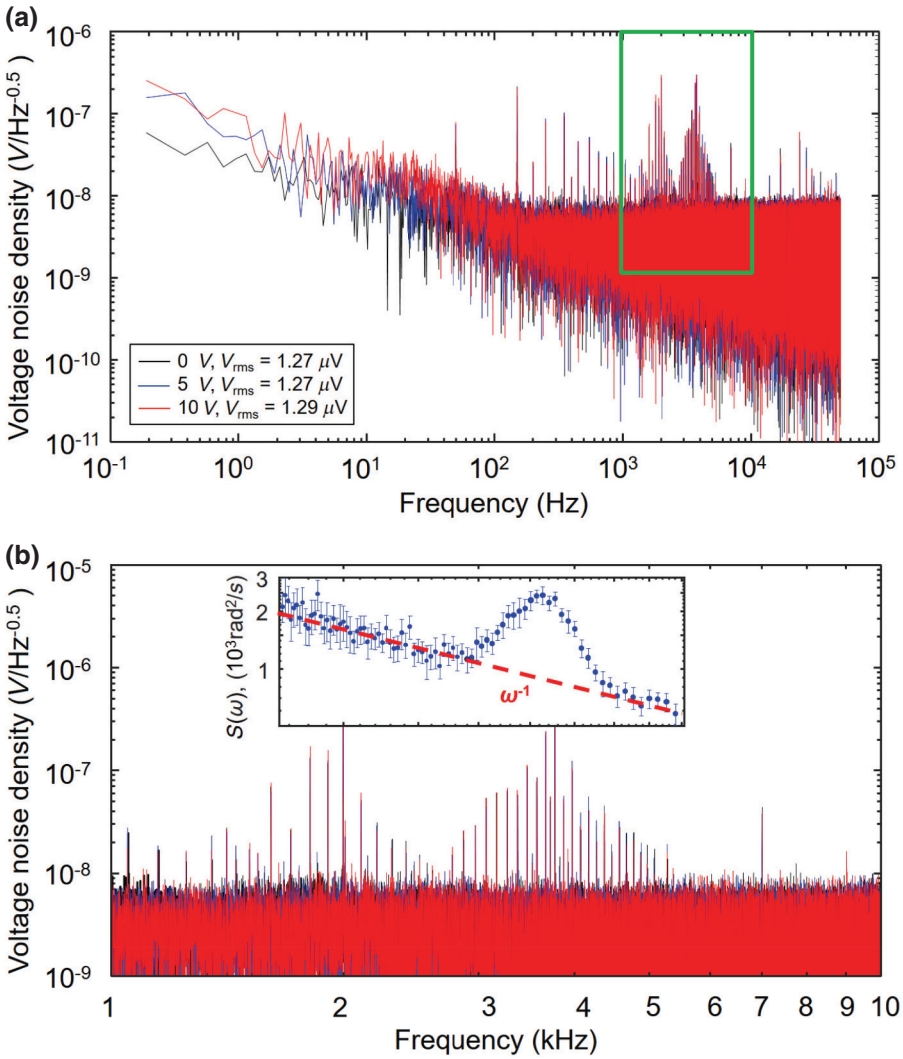

FIG. 5. (a) Measured noise spectrum of the Stanford Research Systems SIM928 dc voltage source used to bias the qubit device. (b) Enlargement of the green region in (a) showing the noise spectrum in the 1–10-kHz range. The inset shows an enlargement of the noise spectrum of Q1 measured with more data points to exemplify the $1/f$ charge-noise trend and corroborate the peak at $f \approx 3.6$ kHz. The plot has the same frequency axis as the SIM928 noise spectrum, showing the matching noise peak at 3.6 kHz.

V. SUMMARY

In summary, we characterize and assess the environment of a silicon quantum dot spin qubit by performing measurements of electron spin-coherence times, Clifford-gate-based randomized benchmarking, gate-induced-Stark-shift measurements, and noise-spectroscopy measurements. Notably, the one-qubit control fidelity in this device is 4 times lower in error rate compared with that in previously reported experiments even though T_2^* is 4 times shorter. We achieve this with better microwave engineering control that includes the use of the vector mode in our microwave source and resonance-frequency feedback control. Our qubit experiences a similar noise environment as the Si:P qubit but we observe a significantly larger influence of $1/f$ noise in the intermediate-frequency range, due to higher sensitivity of our qubits to charge noise, which results from the larger Stark shift present in quantum dot qubits. The peak at 3.6 kHz in the noise spectrum, which is found to be caused by the SIM928 voltage source, should be manageable with proper filtering techniques or alternative measurement electronics. This has emphasized the importance of noise-spectroscopy measurements to probe the sources of noise that are coupled to a qubit. This experiment also highlights the capability of our quantum dot qubits as a sensitive metrological device to detect an electromagnetic noise environment in a nanoelectronic circuit.

ACKNOWLEDGMENTS

We acknowledge support from the Australian Research Council (Grants No. CE11E0001017 and No. CE170100039), the U.S. Army Research Office (Grants No. W911NF-13-1-0024 and No. W911NF-17-1-0198), and the NSW Node of the Australian National Fabrication Facility. K.M.I. acknowledges support from a Grant-in-Aid for Scientific Research by Ministry of Education, Culture, Sports, Science, and Technology, NanoQuine, Funding Program for World-Leading Innovative R&D on

Science and Technology, and the Japan Society for the Promotion of Science Core-to-Core Program.

APPENDIX: SIM928 DC VOLTAGE SOURCE NOISE SPECTRUM

Figure 5(a) shows the noise spectrum of the SIM928 dc voltage source used to bias the qubit device. For this measurement, the SIM928 voltage source is connected to the same type of resistive voltage divider-adder that we use in our setups to combine dc and ac voltage signals. The output of the voltage adder is then fed into an SR560 voltage amplifier and recorded on a digital oscilloscope. The voltage trace is Fourier transformed to obtain the noise spectrum. The three spectra in black, blue, and red are measurements taken with the SIM928 voltage source set to 0, 5 and 10 V, respectively. The noise spectra are independent of the SIM928 voltage, and their average fluctuation for $f = 0.2$ Hz to 50 kHz is $V_{\mathrm{rms}} \approx 1.27\ \mu$V. Figure 5(b) shows an enlargement of the green region in Fig. 5(a), with the inset showing the qubit G1 noise spectrum taken at 1.5–5.5 kHz. Both plots have the same frequency axis, showing the matching noise peak at 3.6 kHz.

[1] Daniel Loss and David P. DiVincenzo, Quantum computation with quantum dots, Phys. Rev. A **57**, 120 (1998).

[2] Juha T. Muhonen, Juan P. Dehollain, Arne Laucht, Fay E. Hudson, Rachpon Kalra, Takeharu Sekiguchi, Kohei M. Itoh, David N. Jamieson, Jeffrey C. McCallum, Andrew S. Dzurak, and A. Morello, Storing quantum information for 30 seconds in a nanoelectronic device, Nat. Nanotechnol. **9**, 986 (2014).

[3] M. Veldhorst, J. C. C. Hwang, C. H. Yang, A. W. Leenstra, B. de Ronde, J. P. Dehollain, J. T. Muhonen, F. E. Hudson, K. M. Itoh, A. Morello, and A. S. Dzurak, An addressable quantum dot qubit with fault-tolerant fidelity, Nat. Nanotechnol. **9**, 981 (2014).

[4] Kevin Eng, Thaddeus D. Ladd, Aaron Smith, Matthew G. Borselli, Andrey A. Kiselev, Bryan H. Fong, Kevin S. Holabird, Thomas M. Hazard, Biqin Huang, Peter W. Deelman, I. Milosavljevic, A. E. Schmitz, R. S. Ross, M. F. Gyure, and A. T. Hunter, Isotopically enhanced triple-quantum-dot qubit, Sci. Adv. **1**, e1500214 (2015).

[5] Alexei M. Tyryshkin, Shinichi Tojo, John J. L. Morton, Helge Riemann, Nikolai V. Abrosimov, Peter Becker, Hans-Joachim Pohl, Thomas Schenkel, Michael L. W. Thewalt, Kohei M. Itoh, and S. A. Lyon, Electron spin coherence exceeding seconds in high-purity silicon, Nat. Mater. **11**, 143 (2012).

[6] Jun Yoneda, Kenta Takeda, Tomohiro Otsuka, Takashi Nakajima, Matthieu R. Delbecq, Giles Allison, Takumu Honda, Tetsuo Kodera, Shunri Oda, Yusuke Hoshi, Noritaka Usami, Kohei M. Itoh, and Seigo Tarucha, A quantum-dot spin qubit with coherence limited by charge noise and fidelity higher than 99.9%, Nat. Nanotechnol. **13**, 102 (2018).

[7] M. Veldhorst, C. H. Yang, J. C. C. Hwang, W. Huang, J. P. Dehollain, J. T. Muhonen, S. Simmons, A. Laucht, F. E. Hudson, K. M. Itoh, A. Morello, and A. S. Dzurak, A two-qubit logic gate in silicon, Nature **526**, 410 (2015).

[8] T. F. Watson, S. G. J. Philips, Erika Kawakami, D. R. Ward, Pasquale Scarlino, Menno Veldhorst, D. E. Savage, M. G. Lagally, Mark Friesen, S. N. Coppersmith, M. A. Eriksson, and L. M. K. Vandersypen, A programmable two-qubit quantum processor in silicon, Nature **555**, 633 (2018).

[9] David M. Zajac, Anthony J. Sigillito, Maximilian Russ, Felix Borjans, Jacob M. Taylor, Guido Burkard, and Jason R. Petta, Resonantly driven cnot gate for electron spins, Science **359**, 439 (2018).

[10] W. Huang, C. H. Yang, K. W. Chan, T. Tanttu, B. Hensen, R. C. C. Leon, M. A. Fogarty, J. C. C. Hwang, F. E. Hudson, K. M. Itoh, A. Morello, A. Laucht, and A. S. Dzurak, Fidelity benchmarks for two-qubit gates in silicon, arXiv:1805.05027 (2018).

[11] Cody Jones, Michael A. Fogarty, Andrea Morello, Mark F. Gyure, Andrew S. Dzurak, and Thaddeus D. Ladd, Logical Qubit in a Linear Array of Semiconductor Quantum Dots, Phys. Rev. X **8**, 021058 (2018).

[12] Jonas Bylander, Simon Gustavsson, Fei Yan, Fumiki Yoshihara, Khalil Harrabi, George Fitch, David G. Cory, Yasunobu Nakamura, Jaw-Shen Tsai, and William D. Oliver, Noise spectroscopy through dynamical decoupling with a superconducting flux qubit, Nat. Phys. **7**, 565 (2011).

[13] Ido Almog, Gil Loewenthal, Jonathan Coslovsky, Yoav Sagi, and Nir Davidson, Dynamic decoupling in the presence of colored control noise, Phys. Rev. A **94**, 042317 (2016).

[14] Y. Romach, C. Müller, T. Unden, L. J. Rogers, T. Isoda, K. M. Itoh, M. Markham, A. Stacey, J. Meijer, S. Pezzagna, B. Naydenov, L. P. McGuinness, N. Bar-Gill, and F. Jelezko, Spectroscopy of Surface-Induced Noise using Shallow Spins in Diamond, Phys. Rev. Lett. **114**, 017601 (2015).

[15] Gonzalo A. Álvarez and Dieter Suter, Measuring the Spectrum of Colored Noise by Dynamical Decoupling, Phys. Rev. Lett. **107**, 230501 (2011).

[16] Tatsuro Yuge, Susumu Sasaki, and Yoshiro Hirayama, Measurement of the Noise Spectrum using a Multiple-Pulse Sequence, Phys. Rev. Lett. **107**, 170504 (2011).

[17] Kohei M. Itoh and Hideyuki Watanabe, Isotope engineering of silicon and diamond for quantum computing and sensing applications, MRS Commun. **4**, 143 (2014).

[18] Susan J. Angus, Andrew J. Ferguson, Andrew S. Dzurak, and Robert G. Clark, Gate-defined quantum dots in intrinsic silicon, Nano Lett. **7**, 2051 (2007).

[19] W. H. Lim, F. A. Zwanenburg, H. Huebl, M. Möttönen, K. W. Chan, A. Morello, and A. S. Dzurak, Observation of the single-electron regime in a highly tunable silicon quantum dot, Appl. Phys. Lett. **95**, 242102 (2009).

[20] Andrea Morello, Jarryd J. Pla, Floris A. Zwanenburg, Kok W. Chan, Kuan Y. Tan, Hans Huebl, Mikko Möttönen, Christopher D. Nugroho, Changyi Yang, Jessica A. van Donkelaar, Andrew D. C. Alves, David N. Jamieson, Christopher C. Escott, Lloyd C. L. Hollenberg, Robert G. Clark, and Andrew S. Dzurak, Single-shot readout of an electron spin in silicon, Nature **467**, 687 (2010).

[21] J. M. Elzerman, R. Hanson, L. H. Willems Van Beveren, B. Witkamp, L. M. K. Vandersypen, and Leo P. Kouwenhoven, Single-shot read-out of an individual electron spin in a quantum dot, Nature **430**, 431 (2004).
[22] Norman F. Ramsey, Experiments with separated oscillatory fields and hydrogen masers, Rev. Mod. Phys. **62**, 541 (1990).
[23] Erwin L. Hahn, Spin echoes, Phys. Rev. **80**, 580 (1950).
[24] Herman Y. Carr and Edward M. Purcell, Effects of diffusion on free precession in nuclear magnetic resonance experiments, Phys. Rev. **94**, 630 (1954).
[25] Saul Meiboom and David Gill, Modified spin-echo method for measuring nuclear relaxation times, Rev. Sci. Instrum. **29**, 688 (1958).
[26] Emanuel Knill, D. Leibfried, R. Reichle, J. Britton, R. B. Blakestad, J. D. Jost, C. Langer, R. Ozeri, Signe Seidelin, and David J. Wineland, Randomized benchmarking of quantum gates, Phys. Rev. A **77**, 012307 (2008).
[27] Easwar Magesan, Jay M. Gambetta, Blake R. Johnson, Colm A. Ryan, Jerry M. Chow, Seth T. Merkel, M. P. da Silva, George A. Keefe, Mary B. Rothwell, Thomas A. Ohki, Mark B. Ketchen, and M. Steffen, Efficient Measurement of Quantum Gate Error by Interleaved Randomized Benchmarking, Phys. Rev. Lett. **109**, 080505 (2012).
[28] Charles D. Hill, Eldad Peretz, Samuel J. Hile, Matthew G. House, Martin Fuechsle, Sven Rogge, Michelle Y. Simmons, and Lloyd C. L. Hollenberg, A surface code quantum computer in silicon, Sci. Adv. **1**, e1500707 (2015).
[29] Robin Blume-Kohout, John King Gamble, Erik Nielsen, Kenneth Rudinger, Jonathan Mizrahi, Kevin Fortier, and Peter Maunz, Demonstration of qubit operations below a rigorous fault tolerance threshold with gate set tomography, Nat. Commun. **8**, 14485 (2017).
[30] Adam Bermeister, Daniel Keith, and Dimitrie Culcer, Charge noise, spin-orbit coupling, and dephasing of single-spin qubits, Appl. Phys. Lett. **105**, 192102 (2014).
[31] Peihao Huang and Xuedong Hu, Electron spin relaxation due to charge noise, Phys. Rev. B **89**, 195302 (2014).
[32] E. Paladino, Y. M. Galperin, G. Falci, and B. L. Altshuler, 1/f noise: Implications for solid-state quantum information, Rev. Mod. Phys. **86**, 361 (2014).
[33] Neil M. Zimmerman, Chih Hwan Yang, Nai Shyan Lai, Wee Han Lim, and Andrew S. Dzurak, Charge offset stability in Si single electron devices with al gates, Nanotechnology **25**, 405201 (2014).
[34] J. Medford, Ł Cywiński, C. Barthel, C. M. Marcus, M. P. Hanson, and A. C. Gossard, Scaling of Dynamical Decoupling for Spin Qubits, Phys. Rev. Lett. **108**, 086802 (2012).
[35] Rifat Ferdous, Kok W. Chan, Menno Veldhorst, J. C. C. Hwang, C. H. Yang, Harshad Sahasrabudhe, Gerhard Klimeck, Andrea Morello, Andrew S. Dzurak, and Rajib Rahman, Interface-induced spin-orbit interaction in silicon quantum dots and prospects for scalability, Phys. Rev. B **97**, 241401 (2018).
[36] J. C. C. Hwang, C. H. Yang, M. Veldhorst, N. Hendrickx, M. A. Fogarty, W. Huang, F. E. Hudson, A. Morello, and A. S. Dzurak, Impact of g-factors and valleys on spin qubits in a silicon double quantumdot, Phys. Rev. B **96**, 045302 (2017).
[37] Arne Laucht, Juha T. Muhonen, Fahd A. Mohiyaddin, Rachpon Kalra, Juan P. Dehollain, Solomon Freer, Fay E. Hudson, Menno Veldhorst, Rajib Rahman, Gerhard Klimeck, Kohei M. Itoh, David N. Jamieson, Jeffrey C. McCallum, Andrew S. Dzurak, and Andrea Morello, Electrically controlling single-spin qubits in a continuous microwave field, Sci. Adv. **1**, e1500022 (2015).
[38] M. J. Biercuk, A. C. Doherty, and H. Uys, Dynamical decoupling sequence construction as a filter-design problem, J. Phys. B: At. Mol. Opt. Phys. **44**, 154002 (2011).